Exploiting Intrinsic Noise to Achieve Heterogeneous Control of Cell Differentiation Dynamics in the Presence of Time Delays, Model Uncertainties, and Extrinsic Variability

M P May[1], B Munsky[1,2]

[1] School of Bioengineering, Colorado State University, Fort Collins, CO, USA
[2] Department of Chemical and Biological Engineering, Colorado State University, Fort Collins, CO, USA

Abstract. Previous research has focused on robust control performance in the presence of noise, but understanding controllers that exploit noise remains incomplete. Motivated by Maxwells-Demon, we previously proposed a difficult control problem which requires the exploitation of noise in a stochastic system to break symmetry between two signals. We found multiple such controllers which could exploit noise to break symmetry between two cells under a variety of system information. This work extends that analysis to include stochastic systems that trace a moving target, are affected by time delay, intrinsic noise, or measurement uncertainty. We find that noise-exploiting controllers can remain highly effective despite coarse approximations to the model's scale or incorrect estimations of key model parameters, and these controllers can even retain performance for significant time delays. Together, these findings suggest that noise-exploiting control should be possible where models are always approximate, where parameters are always uncertain, and where observations are corrupted by errors.
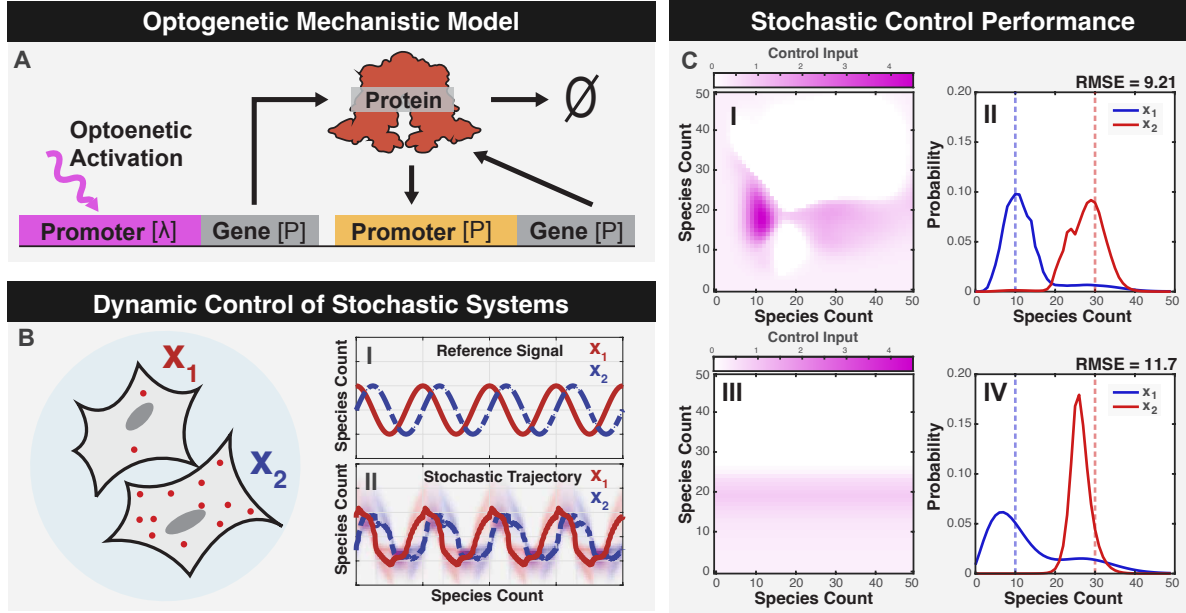
Figure 1. Optogenetic control of multiple cells using a single light input.
(**A**) Schematic of the light activated genetic system with autoregulation. (**B**) Diagram of the stochastic SIMO control problem using two optogenetic cells sharing an input. (**C**) Adapted from (PAPER). Noise exploiting controllers were optimized to a fully aware control input (I), and partially aware control input(III). Marginal distributions are solved using the finite state projection and show a break in symmetry using both controllers (II and IV)

1. Introduction

Uncertain fluctuations, or 'noise,' is a common theme throughout many fields of engineering, and is a frequent concern when attempting to control any human-made system such as vehicles[**?**], production machinery[**?**], or chemical processes[**?**]. Noise arrises from many sources, occasionally from quantum events and thermally-induced fluctuations but more commonly from unknown or uncharacterized physical processes, and as such, these fluctuations usually cannot be efficiently reproduced or predicted using purely physical or mechanistic models. Rather, statistical models are usually employed where key mechanisms or dynamics are subject to stochastic variations or inputs that act as a proxy for random or un-modeled fluctuations elsewhere in the system. In this context, much effort has been placed on enhancing the robustness of controlled processes, where uncertain or unpredictable variations in internal or external parameters are modeled as intrinsic or extrinsic noise [**?**]. For many macroscopic, human-engineered systems, the resulting system dynamics can be modeled effectively simply by combining a deterministic (i.e., noise-free) model with additive noise (usually assumed to be Gaussian under arguments based on the central limit theorem)**??**, and most current approaches seek to control the system to minimize variations that result from the noisy inputs.

Analyses of noise and control theory are equally relevant to understand the basic

biological processes of gene transcription regulation[**?**] or mRNA translation regulation [**?**] or to modify these processes for practical use[**?**]. However, at this mesoscopic scale of cellular biology, where transcription factors compete to activate or deactivate individual genes or where mRNA or protein molecules are present at just a few copies (or none at all) per cell, additive noise model is far less realistic. In this case, Brownian motion, discrete stochastic gene regulation, and noisy mRNA dynamics collectively generate a fundamentally stocastic environment that cells must effectively manage. At this scale, the order or timing of a single reaction event (e.g., the binding of a transcription factor to a promoter) can have dramatic consequences that could last for several cellular generations (e.g., the activation or repression of a gene that promotes unfettered cell growth and differentiation). The cell's drive towards homeostasis requires dealing with the inherently chaotic and noisy processes that reside within it, and despite these challenges, cells generally demonstrate strong capability to survive these noisy processes. When seeking to understand how such systems evolve or react, the central limit theorem and the Gaussian noise may not apply, and a more detailed statistical analysis of probabilistic behavior is needed uncover hidden properties of cellular control mechanisms.

One emerging field that is particularly dependent on the integration of control and noise is synthetic biology, which aims to develop modular[2] and orthogonal [3] components to sense and manipulate [4] complex logical systems, enabling them to exhibit a wide range of advanced biological behaviors[6]. Advances in optogenetics have enhanced the ability to reliably actuate embedded systems within cells, offering the potential to exert precise temporal and spatial control on cellular components[4, 7, 8, 9]. These developments have facilitated computer-programmable regulation of cellular protein production through external optogenetic inputs and smart microscope techniques[10, 11, 12]. These digital-synthetic actuators enable fine-tuned, computer-modulated control of cellular systems, previously unattainable, with faster response times compared to chemical diffusion[13, 7] . Classical and modern control methods like PID control and model predictive control have been implemented in such systems[] to control synthetic systems to different stable points.

While most previous control efforts focussed on deterministic ordinary differential equation (ODE) formulations of the control problem, a few pioneering theoretical works have extended these analysis to include noise and have used stochastic simulations to show how systems can be guided towards unstable points by oscillating around those points [14]. It has recently been shown that new control techniques that leverage the complete probability distribution information of the system could actually harness the noise of single-cell gene regulation to achieve more complicated control objectives. For example, inspired by the genetic toggle switch from Kobayashi et al.[**?**], Szymanska et al. [16] showed that noise could be exploited to achieve independent control of multiple cells using a single input, even despite uncertain parameters or time delays due to maturation of fluorescent proteins or limited observation of the regulatory proteins. In May et al. [1], we identified a simplified stochastic model to reproduce data measured in

Baumschlager, et al.[**?**] for the expression from the XXX promoter under the optogenetic control of a UV-activated T7 polymerase (see model in Figure 1A, top promoter). We then proposed the addition of a positive auto-regulation (Figure 1A, bottom promoter) to help maintain an elevated expression phenotype in the presence of UV excitation, and we demonstrated how a Single-Input-Multiple-Output (SIMO) multicellular controller could control multiple cells to arbitrary phenotypes using only a single input.

This paper extends the analysis of the SIMO multicellular control problem by examining the impact of model uncertainties and fluctuating control objectives on the control performance. These uncertainties include coarse-grained approximations of the system dynamics, errors or extrinsic variations in the system parameter, and time delays between the observation of the cellular dynamics and actuation of the control process. In the following 'Methods' we introduce our formulation of the chemical master equation to analyze the discrete stochastic distribution of cellular responses; we define multiple controllers and demonstrate the computation of their effects on cell dynamics; and we show how the control law can be optimized to improve performance. In the 'Results' section, we explore the how model approximations, parameter inaccuracies, and time delays affect control performance, and we demonstrate a simple scheme for controlling cells to track a dynamically changing reference signal. Using discrete stochastic models based on the chemical master equation, we demonstrate that combining biochemical noise, nonlinear auto-regulation, and a single optogenetic feedback could control two genetically identical cells with different initial conditions to follow different desired trajectories at different frequencies and phases.

2. Methods

In May et al. [1], we developed two models for the description of an optogenetically controlled gene expression system. These first model consisted of six species to describe the light-activated association of two T7 split domains (species 1 and 2) which combine to form an active T7 polymerase (species 3) under optogenetic excitation. The active polymerase could then associate with inactive T7 promoters (species 4), resulting in the formation of an active allele (species 5) that could then transcribe and translated to produce the desired protein product (species 6). The second, much simpler, single-species model was developed by assuming quasi-steady equilibrium for the first five species. Both models were independently parameterized using the same experimental data from Baumschlager et al. [**?**]. Furthermore, an extension was made to each model to incorporate a secondary self-activated promoter-gene construct, where the expression rate was determined by a Hill function 1. Through simulations, we showed that a feedback control law could be designed to force multiple cells to different and individually chosen equilibrium states using a single optogenetic control signal. We also showed that when this control law was parametrized using the simple model, it could be used effectively to control the behavior of the more complicated system, thus demonstrating that control performance could remain high despite inaccuracies in the model. In the

Table 1. Baseline Model Parameters

Parameter	Value	units
κ	0.406	1/min
β	20.0	Molecules
η	8.00	unitless
k_0	0.0001	1/min
γ	0.0203	1/min
u	dynamic	1/min

current work, we adopt the simpler of the two models and extend our analyses to consider the effects of additional model inaccuracies, including coarse-grained model approximations, parameter errors, and time delays, and we also explore the possibility that a single optogenetic control signal could drive the system to track temporally-changing reference signals. Section 2.1 introduces the model; Section 2.2 develops a Master Equation description of the models probabilistic dynamics; Section 2.3 defines a control objective and optimizes that metric to obtain a baseline control law; and finally Sections 2.4 and 2.5 introduces uncertainties into the model related t the granularity of the model approximation or the introduction of time delays, respectively.

2.1. Model

To assess the impact of model approximations on the implementation of noise-enhanced control strategies, we begin with the one-species model proposed by May et al. [1] (Figure. 1A). This model comprises two reactions for production and degradation of the key protein. The nonlinear, UV-dependent production is defined by the following equation:

$$\nu_1(x,t) = \kappa \frac{x^\eta}{x^\eta + \beta^\eta} + k_0 + u(UV(t)), \tag{1}$$

where x is the instantaneous protein level; κ is the maximum strength of the auto-regulation promoter; β is the concentration at which auto-regulation promoter reaches its half maximal strength; η is the cooperativity in the auto-regulation promoter; k_0 is the leakage rate from both promoters; and $u(UV(t))$ is the UV-dependent strength of the T7 promoter. Feedback enables the external modulation of the light input using the state of the system, thereby controlling the T7 promoter strength as a function of state rather than time and eliminating the explicit time dependance in $u(UV(t))$. Protein degradation is assumed to be a first order process with rate γ:

$$\nu_2(x) = \gamma x. \tag{2}$$

All baseline parameters describing the auto-regulation promoter, κ, η, β, and k_0, and the degradation rate γ are presented in Table 1 [1] and are fixed throughout the current study.

2.2. Stochastic analyses of the model

To describe the discrete stochastic behavior of the above model for a population system with N_c cells, we define the current state of the system as the tuple of the non-negative numbers of proteins in each cell: $\mathbf{X}_i = [x_1, x_2, \ldots, x_{N_c}]_i \in \mathbb{Z}_{\geq 0}$, where the index i denotes the enumeration of the state within the countably infinite set of all possible states, $\mathbf{X}_i \in \mathcal{X} = \{\mathbf{X}_1, \mathbf{X}_2, \ldots\}$. The stoichiometry vector, $\mathbf{s}_\mu$, for reaction number μ is then defined as the change in state following that reaction event (e.g., $\mathbf{X}_i \to \mathbf{X}_i + \mathbf{s}_\mu$). Specifically, the $2N_c$ possible reactions are defined in pairs corresponding to production ($\mu \in \{1, 3, 5, \ldots\}$) and degradation ($\mu \in \{2, 4, 6, \ldots\}$) as:

$$
\begin{aligned}
\mathbf{s}_1 &= \mathbf{e}_1, \ \mathbf{s}_2 = -\mathbf{e}_1, \\
\mathbf{s}_3 &= \mathbf{e}_2, \ \mathbf{s}_4 = -\mathbf{e}_2, \\
&\vdots \\
\mathbf{s}_{2N_c - 1} &= \mathbf{e}_{N_c}, \ \mathbf{s}_{2N_c} = -\mathbf{e}_{N_c},
\end{aligned}
\tag{3}
$$

where each $\mathbf{e}_i \in \mathbb{Z}^{N_c}$ is is a Euclidean vector (i.e., unity for the ith entry and otherwise zero). The corresponding propensity functions are:

$$
\begin{aligned}
w_1(\mathbf{X}) &= u(\mathbf{X}, t) + \kappa \frac{x_1^\eta}{x_1^\eta + \beta^\eta} + k_0, \ w_2(\mathbf{X}) = \gamma x_1, \\
w_3(\mathbf{X}) &= u(\mathbf{X}, t) + \kappa \frac{x_2^\eta}{x_2^\eta + \beta^\eta} + k_0, \ w_4(\mathbf{X}) = \gamma x_2, \\
&\vdots \\
w_{2N_c - 1}(\mathbf{X}) &= u(\mathbf{X}, t) + \kappa \frac{x_N^\eta}{x_N^\eta + \beta^\eta} + k_0, \ w_{2N_c}(\mathbf{X}) = \gamma x_N.
\end{aligned}
\tag{4}
$$

These definitions of the stoichiometry and propensity functions allow us to implement the Gillespie stochastic simulation algorithm (SSA) [17, 18] to generate representative trajectories of the stochastic process. At each step two random numbers are generated to determine the time and the type of the next reaction. Given the current state $\mathbf{X}$, the time until the next reaction is distributed according to an exponential random with rate parameter equal to the inverse of the sum of the propensity functions:

$$
Pr(\delta t = \tau) = \sum w_i(\mathbf{X}) \exp\left(-\sum \mu = 1^{2N_c - 1} w_\mu(\mathbf{X}) \tau\right),
\tag{5}
$$

and an instance of this random variable, δt, can be sampled from this distribution using the expression:

$$
\delta t = -\log\left(r_1 \sum_{\mu=1}^{2N_c - 1} w_\mu(\mathbf{X})\right),
\tag{6}
$$

where r_1 is a uniform random variable between zero and one. The probability of for the specific individual reaction R_k to fire from all possible reactions is given by:

$$
Pr(R_k) = \frac{w_k}{\sum w_{\mu=1}^{2N_c - 1}(\mathbf{X})},
\tag{7}
$$

and thus the reaction that fires at time $t + \tau$ is a categorical random variable pulled from $Pr(R_k)$. The SSA is then simulated by stepping through time one reaction at a time and updating the state of the system by adding the stoichiometry of the reaction to the state of the system.

However, a more direct analysis of the chemical master equation (CME) is necessary for performance quantification and optimal controller design. The high dimensional CME is a linear ODE that describes the time-dependent changes in probability mass of all possible states. Using the specified reaction propensities and stoichiometries, the CME can be expressed as:

$$\frac{d}{dt}P(\mathbf{X}_i) = \sum_{\mu=1}^{2N_c} \left(-w_\mu(\mathbf{X}_i)P(\mathbf{X}_i) + w_\mu(\mathbf{X}_i - \mathbf{s}_\mu)P(\mathbf{X}_i - \mathbf{s}_\mu) \right). \tag{8}$$

For convenience, the CME can also be formulated more compactly in matrix-vector form as:

$$\frac{d}{dt}\mathbf{P} = (\mathbf{A}_0 + \mathbf{Bu}^{\mathcal{C}})\mathbf{P}, \tag{9}$$

where $\mathbf{P} = [P(\mathbf{X}_1), P(\mathbf{X}_2), \ldots]^T$ is the enumerated probability mass vector for all possible states of the system; $\mathbf{A}_0$ is the infinitesimal generator of the stochastic process due to the autoregulation promoter and degradation events; $\mathbf{u}^{\mathcal{C}} = [u^{\mathcal{C}}(\mathbf{X}_1), u^{\mathcal{C}}(\mathbf{X}_2), \ldots]^T$ is the collection of control inputs associated with each state; and $\mathbf{Bu}^{\mathcal{C}}$ is the contribution that these control inputs make to the infinitesimal generator when included into the feedback process.

More specifically, the zero-control infinitesimal generator, $\mathbf{A}_0$, is constructed according to:

$$[\mathbf{A}_0]_{ij} = \begin{cases} -\sum_{\mu=1}^{2N_c} w_\mu(\mathbf{X}_j), & \text{for } i = j, \\ w_\mu(\mathbf{X}_j), & \text{for } \mathbf{X}_i = \mathbf{X}_j + \mathbf{s}_\mu \\ 0, & \text{otherwise}, \end{cases} \tag{10}$$

and the feedback infinitesimal generator, $\mathbf{Bu}^{\mathcal{C}}$, of the controller is constructed according to

$$[\mathbf{Bu}^{\mathcal{C}}]_{ij} = \begin{cases} -N_c u^{\mathcal{C}}(\mathbf{X}_j), & \text{for } i = j \\ u^{\mathcal{C}}(\mathbf{X}_j), & \text{for } \begin{aligned} &\mathbf{X}_i = \mathbf{X}_j + \mathbf{e}_{i_c}, \\ &\text{and } i_c = 1, \ldots, N_c \end{aligned}, x \\ 0, & \text{otherwise}, \end{cases} \tag{11}$$

where $u^{\mathcal{C}}(\mathbf{X}_j)$ is the specification of the controller, $\mathcal{C}$, in terms of the current instantaneous state, or its partial observations.

For a given controller, the equilibrium distribution of the system ($\mathbf{P}^*$) can be found by solving Eq. 9 and is given by:

$$\mathbf{P}^* = \text{null}(\mathbf{A} + \mathbf{Bu}^{\mathcal{C}}). \tag{12}$$

In principle, the master equation in Eq. 9 could contain an uncountably infinite number of states, and therefore the exact solution as well as the null vector in Eq. 12

may not be computable exactly. To address this issue, we first truncate the system at a finite number for each species and then apply a reflecting boundary condition, resulting in a finite dimensional master equation. To assess the time interval over which this truncation is valid, we also solve the Finite State Projection[**?**] for the same truncation, which allows us to compute an upper bound on the truncation error as a function of time.

We should use the FSP to compute the error of the truncation for a couple cases. We can talk about how to do this when we meet. ok!

2.3. Quantification and optimization of control performance

In the SIMO control of stochastic processes, a single input is applied simultaneously to all systems at once and a control signal that acts beneficially on one system destabilizes other systems. Stochastic SIMO control inputs which seek to control cells one-cell-at-a-time create increased instability and response variability in the other signals not being controlled. Thus, even in systems which do a good job at controlling a system cannot independently control individual cells to a desired target point without impacting the variance of others, so an effective controller must strike a balance among the desired behaviors of all cells in the system.

To quantify performance success, we define the *steady state performance error*, J, as the expected steady state Euclidean distance of the process from the specified target state, $\mathbf{T}$:

$$J = \mathbb{E}\{|\mathbf{X} - \mathbf{T}|_2\}. \tag{13}$$

The squared score is easily calculated by applying a linear operator on steady state probability distribution $\mathbf{P}^*$ (Eq. 12) as follows:

$$
\begin{aligned}
J^2 &= \lim_{t \to \infty} \mathbb{E}\{|\mathbf{X}(t) - \mathbf{T}|_2^2\}, \\
&= \sum_{i_1, i_2, \ldots} P^*(x_1 = i_1, x_2 = i_2, \ldots) \left[(i - T_1)^2 + (j - T_2)^2 + \ldots\right], \\
&= \mathbf{C}\mathbf{P}^*,
\end{aligned}
\tag{14}
$$

where $\mathbf{C}$ is simply a vector that contains the squared Euclidian distance of each state from the specified target T, i.e., $C_i = |\mathbf{X}_i - \mathbf{T}|_2^2$. As a result of this calculation, J is a non-negative scalar that is zero if any only if $\mathbf{P}^*$ is a delta distribution located exactly at the target vector $\mathbf{T}$.

We consider two controller designs: the fully aware controller ($\mathbf{u}^{FAC}$) that bases its control signal on simultaneous protein count observations from both cells, and the partially aware controller ($\mathbf{u}^{PAC}$) that relies only on observations from a single cell:

$$\mathbf{u}^{FAC} = u(x_1, x_2), \tag{15}$$

$$\mathbf{u}^{PAC} = u(x_2), \tag{16}$$

where x_1 and x_2 are discrete integers greater than or equal to zero that represent the number of proteins in cell one and cell two. Despite their differences in their observation

data, both the FAC and the simpler PAC are optimized to achieve the same goal, namely to drive both cells to their respective set points.

Optimization of $\mathbf{u}^{FAC}$ was performed using a gradient descent method to minimize J. Since the square root is a monotonically increasing function, minimizing J^2 results in the same control as would minimizing J directly. Therefore, we calculate the negative gradient $-\frac{d(J^2)}{d\mathbf{u}^{FAC}}$ and walking in a small step du in that direction. The calculation of the gradient is given by

$$\frac{d(J^2)}{d\mathbf{u}^{FAC}} = C\frac{dP}{d\mathbf{u}^{FAC}} \tag{17}$$

Where $\frac{dP}{d\mathbf{u}^{FAC}}$ can be solved using general minimized residual calculation of

$$A\frac{dP}{d\mathbf{u}^{FAC}} = B\mathbf{u}^{FAC} \tag{18}$$

to find $\frac{dP}{d\mathbf{u}^{FAC}}$.

In [1], controllers were optimized to minimize J^2 for a single target state $\mathbf{T} = [10, 30]$, but in this work they are extend to different arbitrary target points.

2.4. Scaling for system granularity

In realistic applications, models are never exact, but are often chosen as simplifications of known processes. For example, when analyzing discrete stochastic chemical kinetics, it is common to project the CME onto lower-dimensional spaces using finite state projection[?], time scale separations [?], Krylov subspaces [?], principle orthogonal decompositions [?], or other coarse meshes [?, ?]. Similarly, measurements are also always inexact and in many cases may only provide information about relative changes – for example, although fluorescent proteins usually cannot be counted exactly, one may reasonably assume that a cell's total fluorescence intensity varies linearly with the fluorescent protein concentration. To explore how mismatches in assumed system scale (e.g., arising from model approximations or relative measurements) affect the controllability of the cellular process, we define a granularity parameter ($\alpha = M'/M$) that linearly scales each species' population to increase ($\alpha > 1$) or decrease ($\alpha < 1$), while maintaining the dynamics and general behavior of the model. To apply this granularity parameter, we assume that each propensity function, w_μ (Eqns. 4) is rescaled to a different level of discreteness by substituting

$$w'(\mathbf{X}) = w(\mathbf{X}/\alpha). \tag{19}$$

For example, the production and degradation of protein in cell one would become:

$$w'_1(\mathbf{X}) = u(\mathbf{X}/\alpha, t) + \kappa\frac{(x_1/\alpha)^\eta}{(x_1/\alpha)^\eta + \beta^\eta} + k_0$$
$$w'_2(\mathbf{X}) = \gamma x_1/\alpha. \tag{20}$$

We note that in order to reuse a control law that has been defined for one level granularity and apply it to a system at another level of granularity, the inputs to the controller must also be scaled by $1/\alpha$ before computing the control level assigned to the current

state, e.g., $u^{\mathcal{C}} = u^{\mathcal{C}}(\mathbf{X}/\alpha)$. Because identification of the original control formulation, $\mathbf{u}^{FAC}(x_1, x_2)$ and $\mathbf{u}^{PAC}(x_1)$ only considered integer values for (x_1, x_2), control signal values at fractional state values after rescaling $(x_1/\alpha, x_2/\alpha)$ are calculated using 2D cubic interpolation from the control values at the nearest integer state values. Finally, to provide a consistent metric for relative scoring, the definition of the performance score is also adjusted according to scale magnitudes. For example, in the two cell system the new steady state performance error would become:

$$
\begin{aligned}
(J^2)' &= \sum_{i=0}^{M'} \sum_{j=0}^{M'} P^*(x_1 = i, x_2 = j)((i/\alpha - \mathbf{T}_1)^2 + (j/\alpha - \mathbf{T}_2)^2), \\
&= \mathbf{C}'\mathbf{P}^*.
\end{aligned}
\tag{21}
$$

We reiterate that the system parameters and control law were defined and fixed using the the base granularity ($\alpha = 1$), and these are not recomputed or refit upon changing the system granularity.

2.5. Observation and actuation time delays

Delays are inherent in any realistic control systems, and it this case delays would be expected to arise due to the time needed for various biochemical reactions such as formation of complete polymerases, activation of promoters, transcription and transport of mature mRNA, and the translation and maturation of protein [?]. Additional delays would also arise from data analysis, decision making, and actuation dynamics. To investigate the effects of time delay on control actuation, we devised a simple time-delay stochastic simulation algorithm. This algorithm records the state history after each stochastic jump, enabling reconstruction of the population history of the species and the time delayed control input propensity. Using this information, the time-delayed control signal at time t can be specified as:

$$
u_\tau(t) = \begin{cases} 0, & \text{for } t \le \tau, \\ u^{\mathcal{C}}(x_1(t - \tau), x_2(t - \tau)), & \text{for } t > \tau, \end{cases}
\tag{22}
$$

where τ is the time delay between observation and actuation, $u^{\mathcal{C}}$ is the previously optimized control law (e.g., $\mathbf{u}^{\text{FAC}}$ or $\mathbf{u}^{\text{PAC}}$), and x gathered from the state history. Explain how you modify the SSA for the delayed reaction SSA. Look through the literature to cite someone else who has implenented a similar method. We note that the time delay stochastic process was only simulated using the SSA because to our knowledge an appropriate direct FSP/CME integration procedure has not yet been developed.

2.6. Dynamic Setpoint Control

Because optimizing the control law for a static set point as described in Section 2.3 requires differentiation of the CME (Eq. 9) with respect to the control signal at each state, this calculation is approaching the limits of current feasibility. Extending

these calculations to optimize controllers for a dynamically moving set point is much harder and would likely require intractable numerical simulation or development of new mathematical approaches that are beyond the scope of the current study. To circumvent this challenge, we instead propose a simple alternative to sweep though a set of controllers over time which target different static points in piecewise fashion to mimic a dynamically moving path.

We start by describing a discrete path of target points in state space which cycle at fixed frequency. Then, we optimize controllers for each target point and cycling through the controllers over time to create the final controller $\mathbf{R}(\mathbf{x}, t)$. Let $\mathbf{p}(t)$ be a continuous and cyclicly moving point in state space

$$\mathbf{p(t)} = [x_1(t), x_2(t)] \tag{23}$$

where $x_1(t)$, and $x_2(t)$ are both cyclic functions of time $\in \mathbf{R}$. Then, $\mathbf{q}$ is a collection of points q_i which evaluate the cyclic function over its natural period (T) in n steps.

$$\mathbf{q} = [q_1, \ldots, q_n] = [\mathbf{p}(t_1), \ldots, \mathbf{p}(t_n)] \tag{24}$$

where each t_i comes from linearly spaced points between 0 and T, in n steps

$$t_i = [t_1, \ldots, t_n] = [0, \frac{1}{n}T, \ldots, \frac{n}{n}T] \tag{25}$$

Then, we optimize a set of controllers which target each q_i in the discretized path.

$$\mathbf{U}_i(\mathbf{x}) = [\mathbf{u}_1(\mathbf{x}), ..., \mathbf{u}_n(\mathbf{x})] \tag{26}$$

Next, we cycle through each controller at a fixed frequency by using $(\phi(t))$.

$$\phi(t) = \lceil \frac{n}{T} mod(t, T) \rceil = \lceil n \ f \ mod(t, \frac{1}{f}) \rceil \tag{27}$$

where f the cycling frequency given by $1/T$. Then the final control equation is given by

$$\mathbf{R}(\mathbf{x}, t) = \mathbf{U}_{\phi(\mathbf{t})}(\mathbf{x}) \tag{28}$$

Where $\mathbf{R}(\mathbf{x}, t)$ returns the control input scalar as a function of state and time. The dynamical system equation becomes

$$\frac{d}{dt}\mathbf{P} = \mathbf{A} + \mathbf{B}\mathbf{R}(\mathbf{x}, t) \tag{29}$$

Since $\mathbf{R}(\mathbf{x}, t)$ is a function of time, the system is no longer time invariant.

3. Results

We still need this. Add a paragraph or two to explain the big picture here. Use figure 1 to remind the reader of (1) the control goals, (2) the control law, (3) the resulting distributions, (4) the objective function and (5) the optimization of the control law to minimize the error. Refer to the methods for each such calculation. This section is critical to make sure the reader understands what is coming next. Then provide an outline of the remaining subsections of the results section so that the reader knows what to expect.
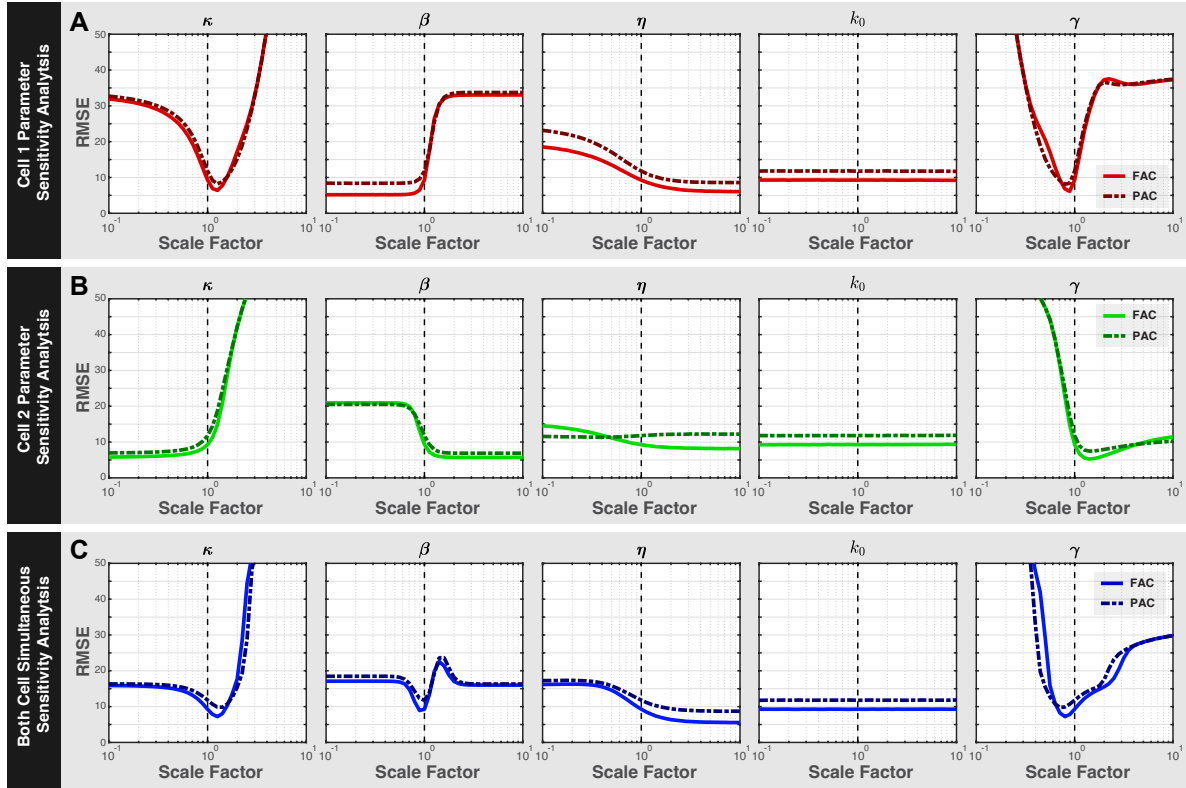
Figure 2. Parameter sweeps using the FAC and PAC show a broad range of control performance in cell 1 (**A**), in cell 2 (**B**), and in both cells (**C**). Columns show each parameter in the model, rows show the cell which has its parameter perturbed.

new paragraph here

In this section, we seek to show that noise-exploiting controllers are effective at controlling a noisy system to a dynamically moving target point. To do this, we show that control performance is robust to a range of parameter uncertainties without the needing adjustments to the controller. Then, we extend the control performance analysis to understand how time delay and system scale alters control performance. Furthermore, we find regions in target space which are easiest to control by optimizing individual controllers for each target. We extend these analysis to change the target point over time in a Peicewise fashion.

3.1. Stochastic SIMO Optogenetic Control can Remain Effective Despite Small Parameter Errors or Extrinsic Uncertainties

Real stochastic processes always have unknown or uncertain mechanisms and parameter values. Although model structures and parameter estimates can often be obtained through fitting to training data, these estimates will never be perfect due to unavoidable measurement errors or limited data sets. Even with plentiful and precise training data, model and parameter uncertainties are inevitable due to the fact that even genetically identical single-cells exhibit heterogeneity in parameters due to extrinsic variations. To

asses the control performance under such parameter errors, we performed sensitivity analysis on each model parameter for each cell, then on both cells simultaneously. For each parameter, $\mathbf{u}^{\text{FAC}}$ (solid lines) and $\mathbf{u}^{\text{PAC}}$(dashed lines) control performance was examined across a parameter perturbation range from one-tenth to ten-fold of the original values. Figure 2A shows the results for these parameter sweeps when a single parameter in Cell 1 is varied (all other parameters are fixed), and Figure. 2B shows the control performance as single parameters in Cell 2 is varied. Finally, 2C shows the performance change when a single parameter is changed simultaneously in both Cell 1 and Cell 2 at the same time.

Modification of parameters were found to produce a broad range of effects. For example, increasing β in Cell 1 quickly worsens performance while increasing β in Cell 2 improves performance (compare second column in Figure. 2A and 2B). In some cases, the effects on performance are not monotonic; for example, increasing κ in Cell 1 (Figure. 2A, leftmost column) would be highly advantageous up to a limit after which the control performance degrades rapidly. In other cases (such as for the promoter leakage rate, k_0), the effect of parameter perturbations on performance is insignificant even for relatively large ($s=10$) perturbations, suggesting that this parameter is not important to control performance. Figure 2C shows that even when parameters of both Cell 1 and Cell 2 are jointly changed, these changes could also improve or detract from control performance. In particular, the analysis shows that control performance could be improved by modifying the system design either to increase the auto-regulation promoter strength (κ) or its cooperativity (η) or to decrease the promoter binding constant (β) or the protein degradation rate (γ).

3.2. Controllers trained using one assumed level of granularity can remain effective at other levels of granularity.

We next explored how the granularity of the system would affect the differential control of the process. Specifically, we define the level of granularity using the parameter α as described in Section 2.4 and which affects the propensity functions and scoring according to equations 19-21. Effectively, larger α corresponds to systems where larger numbers of individual molecules are needed to achieve the same concentration (e.g., larger volumes), while smaller α corresponds to smaller population sizes (e.g., smaller volumes). We previously optimized the controllers $\mathbf{u}^{\text{FAC}}$ and $\mathbf{u}^{\text{PAC}}$ based on a the default assumption that $\alpha = 1$, and we wished to know what would be the consequences if this same controller were to be applied to a system that has a different granularity.

To explore this tradeoff, control performance scores for the $\mathbf{u}^{\text{FAC}}$ and $\mathbf{u}^{\text{PAC}}$ controllers were calculated at different levels of granularity (α) between 0.2 and 2.0. Figure 3 (A - F) shows the joint probability distributions (left plots) and marginal probability distributions (right plots) of the system at a low granularity ($\alpha = 0.2$), the original granularity ($\alpha = 1.0$), and at an increased granularity ($\alpha = 2.0$). Figure 3G shows the trend of the performance versus alpha for both the FAC (solid cyan line)

and the PAC (solid magenta line) controller. This improvement in performance appears to approach a small value as the granularity goes to infinity, but since the size of the FSP increases with the square of the system size, systems much larger than $\alpha=2$ (where $\mathbf{A}_0 \in \mathbb{R}^{10^4 \times 10^4}$) become more difficult to calculate using master equation techniques. To bypass this limit in the FSP, sixteen SSA simulations were used to sample the CME of a system with a much larger volume of $\alpha=100$. Each SSA was ran for 5×10^7 minutes and only the last 4×10^7 minutes were sampled to estimate the stationary distribution and calculate the performance score. The performance score estimates of this high granularity SSA using the FAC and PAC were 2.03 and 5.24 respectively, which are plotted as dashed lines in Figure. 3G. Although it is unclear if further performance improvements could be obtained with further increases to the system scale, for all cases considered so far, we found that both controllers monotonically improved with increased α and that $\mathbf{u}^{\mathrm{FAC}}$ always outperforms the $\mathbf{u}^{\mathrm{PAC}}$.

The effect that granularity has on the control performance depends on two competing phenomena: First, because the controller was optimized for one level of granularity ($\alpha = 1$), one might expect that the controller would become worse if the granularity were incorrect. However, at large granularity, we find that the opposite is true - the control performance actually improves when applied to an incorrect model. The reason for this surprising result is that relative amplitude of stochastic fluctuations (i.e., the standard deviation divided by the mean) in a chemical process decreases with the inverse square root of the process scale [?]. In other words, the process become more predictable and therefore more controllable. At the extreme as the system size increases, the dynamics converge towards a deterministic process, except for certain exceptional initial conditions lying on manifolds that would separate different steady state behaviors [?].

However, the improvement in the steady state performance does not come without a cost. Although higher granularity reduces noise and makes it easier to maintain desired states once they have been achieved, noise is necessary to break symmetry between the two cells' dynamics to achieve those states in the first place. This tradeoff is illustrated in Figure3(H), which plots the control performance over time after the changing the controller goal to exchange the low- and high-target cells with one another. From the figure, we can see although steady state control performance improves for higher values of α, the time taken to reach that steady state performance increases also increases α.

3.3. Heterogeneous control can remain effective despite moderate time delays

In general, feedback control can only be effective if one can quickly make measurements, compute adjustments to the control signal, and implement the needed changes within an appropriate amount of time relative to the characteristic times scales of the system. As the time required for any of these steps increases, control performance will be degraded, perhaps even leading to large fluctuations or instability. To explore how time delays would affect the noise-enhanced controllers $\mathbf{u}^{\mathrm{FAC}}$ and $\mathbf{u}^{\mathrm{PAC}}$, we generated large sets of
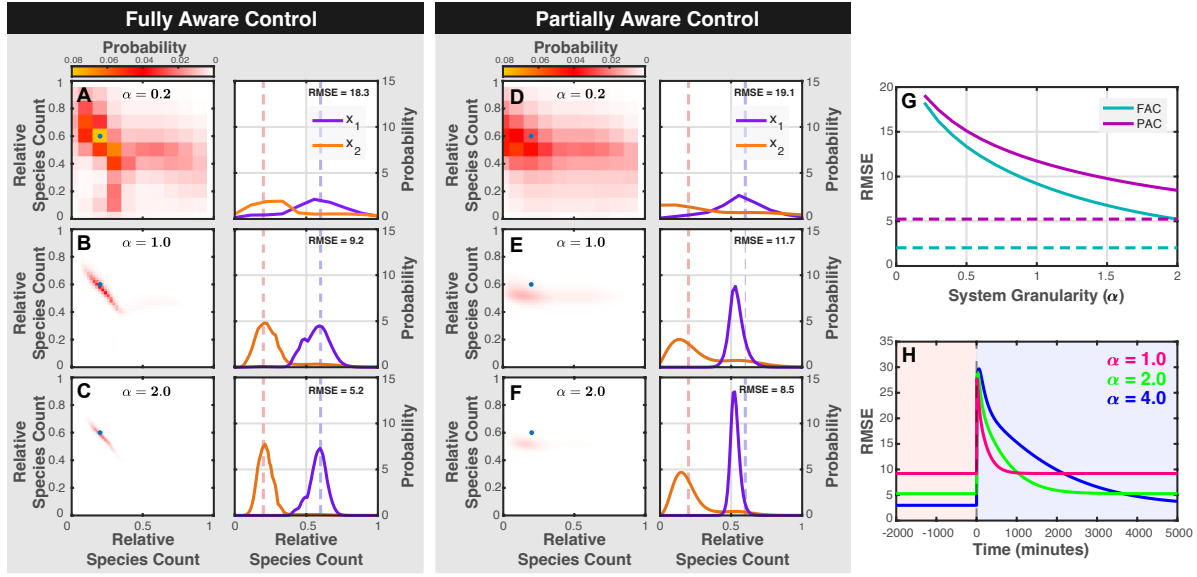
Figure 3. Systems with increased granularity are less noisy and have better control performance. (A-C) Joint (left) and marginal (right) distributions for the FAC shows increased control performance and tighter distributions as α increases from 0.2 (top row) to 2.0 (bottom row) . (D-F) Joint (left) and marginal (left) distributions using the PAC controller at different levels of granularity.
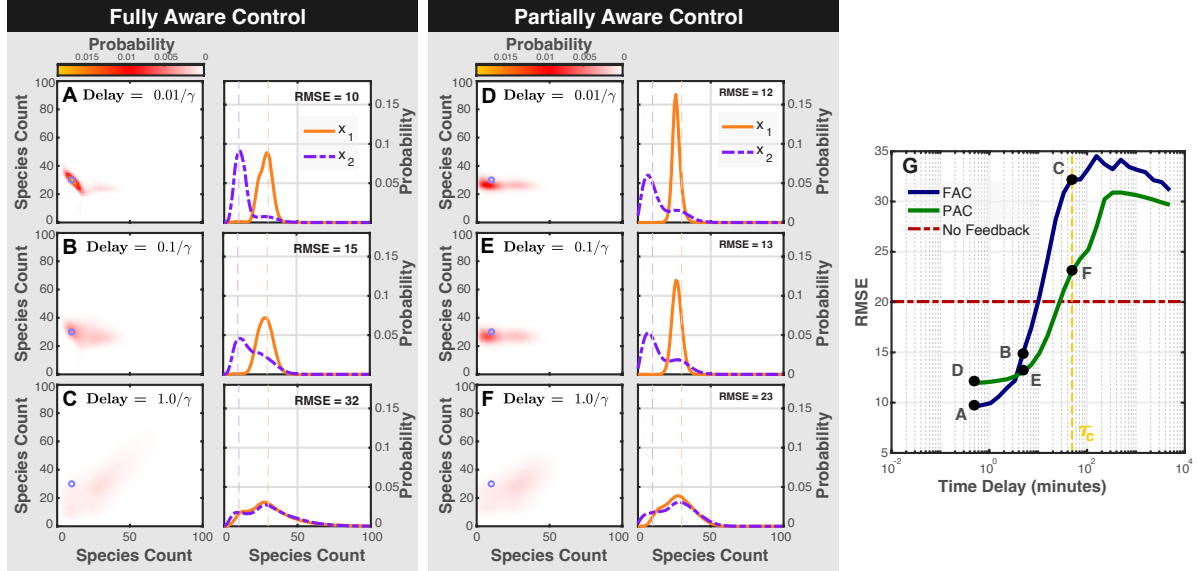

Figure 4. Stochastic simulations of the time delayed system show decreasing control performance using either the FAC or PAC. (A-C) Joint (left) and marginal distributions (right) of the at different levels of time delay for the FAC. (D-F) Joint (left) and marginal distributions(right) at three levels of time delay using the PAC. (G) plots of RMSE control performance versus time delay for both FAC and PAC.

time-delayed stochastic simulations (see Methods) for different lengths of the time delay. Each SSA was sub-sampled for 1000 times over 10000 minutes of simulation time after

a burnin period of 10000 minutes.

Figure 4 shows the joint distributions (left) and marginal distributions (right) at varying levels of time-delay, with panels A-C showing results for the FAC controller and panels D-F showing results for the PAC controller. Figure 4G summarizes these results by plotting the score of both controllers versus the time delay. From the figures, it is clear that performance is rapidly degraded as the delay approaches and then exceeds the characteristic time scale ($\tau_c = 1/\gamma = 49$ min) set by the degradation rate of the process (yellow dashed line). At very small time delays ($\tau < 3.4$ min), the FAC outperforms the PAC but at moderate time delays ($\tau > 3.4$) the PAC outperforms the FAC.

Are these times correct? Isn't gamma = 0.0203 in Table 1? tau = 0.07 / 0.0203 (1/min) = 3.44 min. Please check this carefully. I changed characteristic tau to be 1 since it fits all the curves the best What are the units in Figure 4G? minutes

These data show that time delays greater than $\tau = 0.1/\gamma = 4.9$ min begin to degrade FAC control performance and plateau at $\tau_c = 1.0/\gamma = 49$ min. Check these times. rewrote the sentence The choice of best controller depends on the level of time delay in the system. At extreme time delays, both controllers lose their asymmetry, resulting in significantly worse scores ($RMSE = 32$ and 23). The control performance of simple constant control input without feedback was better than both controlers at very large time delays. Figure4(G) (red line) and achieved a score of $J = 20.0$. These findings indicate that, for large time delays, attempting to improve control with feedback is less effective than using a no-feedback approach.

As discussed in the previous section, increasing the granularity of the system α reduces the randomness to improve the steady state performance but at the cost of slowing down the controller response. To explore the joint effects of time delays and granularity, Fig, 5J shows the FAC steady state control performance as a function of the time delay and system granularity (τ, α) using thirty-two stochastic simulations simulated to steady state at each combination. Control performance errors measured by RMSE improved as α increased when the delays were small ($\tau = 1$ min and $\tau = 10$ min) but not when $\tau = 100$ min.

What are the units of tau in Figure5? This section is confusing in that it is not clear to me how tau and gamma are changing relative to one another when alpha is changed. From Eq 21 it seems that gamma changes with 1/alpha. If this is correct, does that mean that the critical time changes with $\tau_c = 1/gamma = alpha/gamma = 5*alpha$? If you plot that as a thick dashed dark line in Figure5J, would it match to the contours? $tc = 1/(0.7 * alpha)$ matches the counters well

Recalling that under the system granularity rescaling (Eq. 20), as α changes, the effective degradation rate scales according to $\gamma' = \gamma/\alpha$. Therefore, the critical limit for the delays should also change with the system scale according to $\tau_c = 1\alpha/\gamma$. Figure5(J) depicts this characteristic line and shows that as the time delay approaches and then exceeds this level, the steady state performance become dramatically worse. edited this section

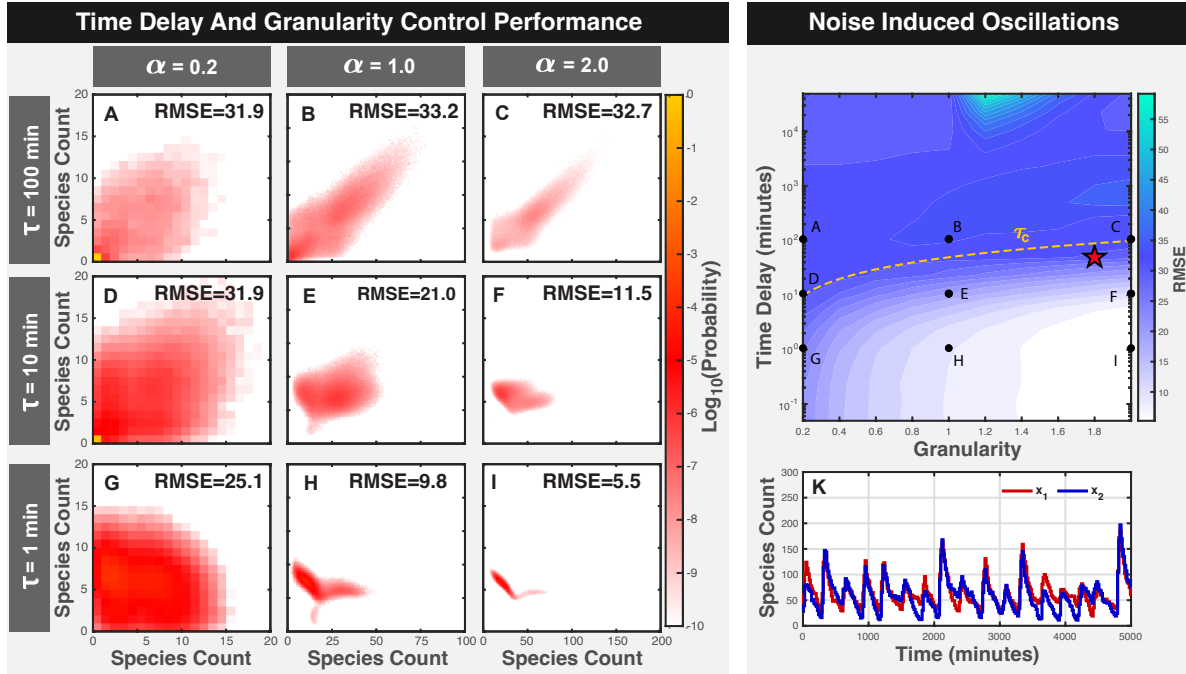Finally, to understand the model of failure at these longer delays, it is interesting

Figure 5. Stochastic simulations of the FAC driven system and PAC driven system show different failure modes at at different (τ, α) pairs. (A-I)Joint probability distributions at different $[\tau, \alpha]$ pairs. α across columns and τ across rows. (J) Control performance measured over a domain of (τ, α) pairs show good control performance when both α is large and τ small. (K) Trajectories where good control was expected but not observed show oscillations instead.

to examine trajectories induced by the controller just above this characteristic delay. For parameter set denoted by the yellow start in Figure. 5(J), Figure. 5(K) shows the controlled response after a long burn in period to achieve steady state. In this case, the application of feedback after a delay leads to a strong oscillatory behavior and worse performance than that achieved without any control at all. This observation further stresses the importance of considering time delays when designing such controllers.

3.4. With noise-induced control, a single input can drive multiple cells to follow different temporal trajectories.

We next optimized the FAC controller and calculated its performance for the two-cell system over a two dimensional domain of target points $[T_1, T_2]$ between between five and forty-five. For example, Figure6 (A) shows the optimized FAC control input of the system when the target is $\mathbf{T} = [20, 25]$, and Figure. 6 (B) shows the corresponding steady state probability distribution of the controlled system. Figure 6 (C and D) show the the same thing but for a different target state of $\mathbf{T} = [10, 25]$.

Let's remove the PAC from this section. Show only the FAC and and replace the Figure6C/D with the FAC at a different target point. Put a new star of a different color to match to the new 6C/D. Remove Figure6F. Make sure to change all the figure labels
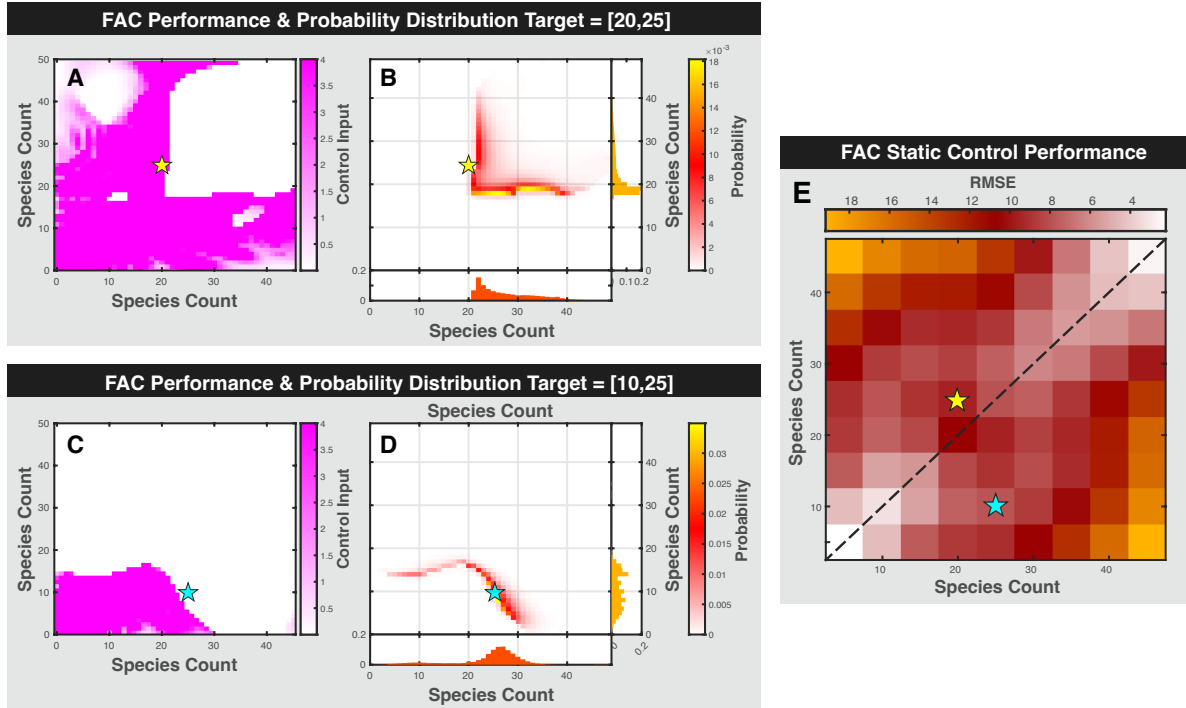
Figure 6. The FAC and PAC control methods were used to optimize control inputs and probability distributions for static set points in a 2D domain. Optimized control inputs and probability distributions were optimized using the FAC control method(A and B) or the PAC control method (C and D). (E) Domains of control performance for the FAC method over a region of static target points show regions of good control and symmetry along the dashed line.

and titles and captions. ok, I also moved the settpoint score heatmap to the right

Figure 6(E) shows the FAC control performance over the entire domain of static set points, and illustrates that some regions are easier to obtain than others. For example, in the space contained in the dashed-green box which also hold the four stable points of the system, the control performance is quite strong, whereas near the unstable point (dashed-blue box), the FAC results in relatively worse control.

The top left and bottom right edge regions were the most difficult to control, since the control input does not push probability in these directions. I don't understand this statement. editied it better

We developed a method (Section 2.6) to control the system dynamics to follow a predefined path $p(t)$. Specifically, three controllers were optimized along three representative pathways in thirty-two steps each, which include an in-sync reference point (Figure. 7B1), a phase lagged reference point (Figure. 7C1), and a frequency separated reference point (Figure. 7D1). The synchronous signal is given by Figure 7(B1) $p_1(t) = [20sin(2\pi ft)+10, 20sin(2\pi ft)+10]$, the phase lagged signal Figure 7(C1) is given by $p_2(t) = [20sin(2\pi ft)+10, 20cos(2\pi ft)+10]$, and the frequency changed signal Figure 7(D1) is given by $p_3(t) = [20sin(2\pi ft)+10, 20sin(6\pi ft+3\pi)+10]$ using 32 steps for each controller.
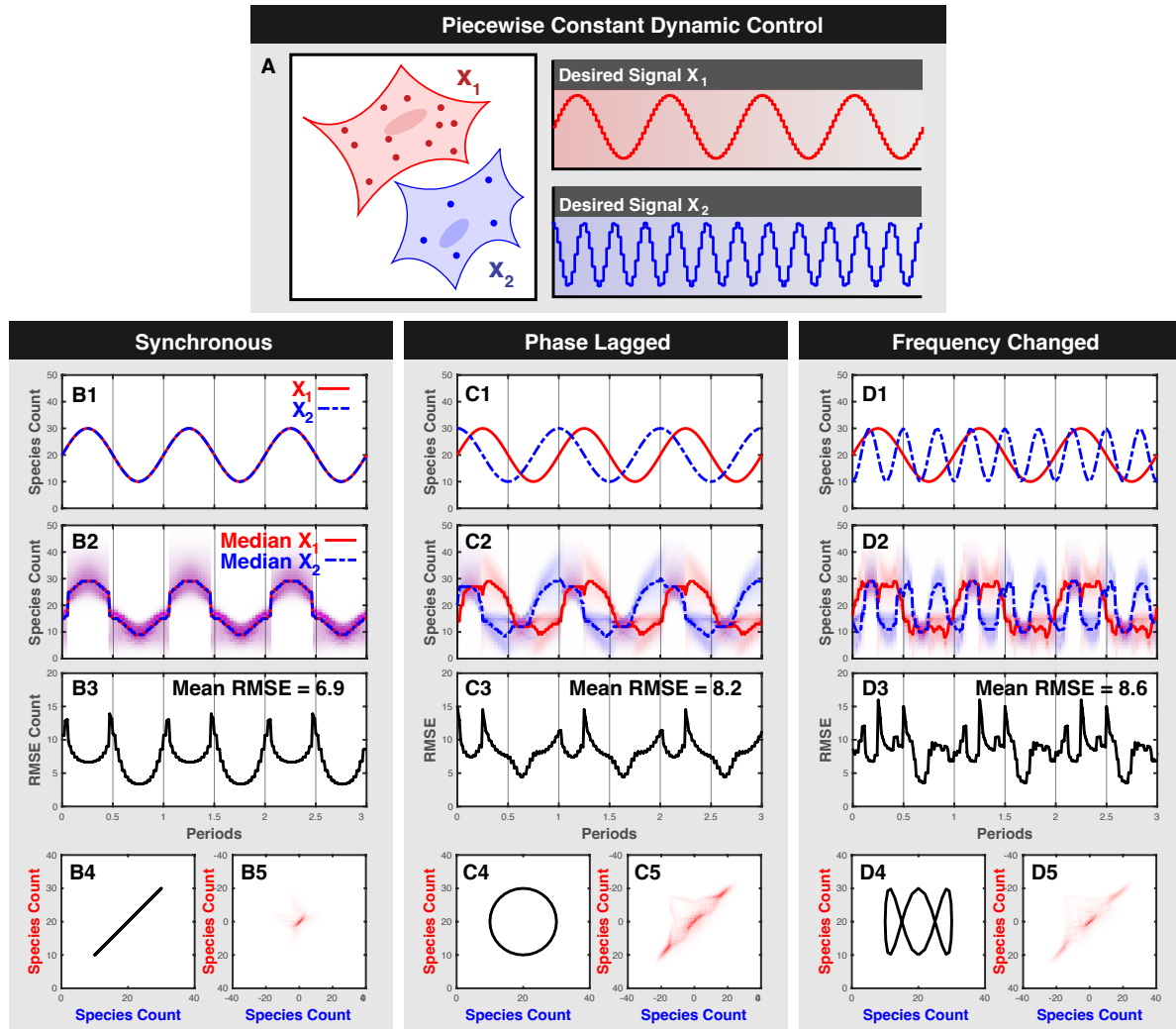
Figure 7. Finite state projections of the slowly driven system demonstrate good control performance under a variety of phase and frequency scenario. (A) Schematic of the control problem shows targeting the number of protein in two cells using a dynamically changing reference point by cycling through a set of individual stable points and under synchronous, phase-lagged or frequency changes reference signal using only one control input. (B1-BN) shows the phase space of the reference time series, FSP solution, RMSE, reference phase space, and error residuals respectively for the synchronous control method. (C1-C5) Shows the same data for the phase-lagged control input. (D1-D5) Shows the same analysis for the frequency-changed control.

All FSP simulations were slowly driven at a frequency of $1e^{-4}min^{-1}$ Check units. This doesn't make sense. did you mean period? If so, this is very fast. Or did you mean s^{-1}? it was min^{-1} not s and Figure. 7(B2, C2, and D2) show their response distributions (shading) and median responses (lines) for the two cells x_1 and x_2 in red and blue, respectively. Regions with purple shading depict the exact overlap of red and blue when both cells have the same distribution of response. We observe that the single-input control system is able to effectively control the system to follow all three input trajectories, including when the two reference trajectories have different
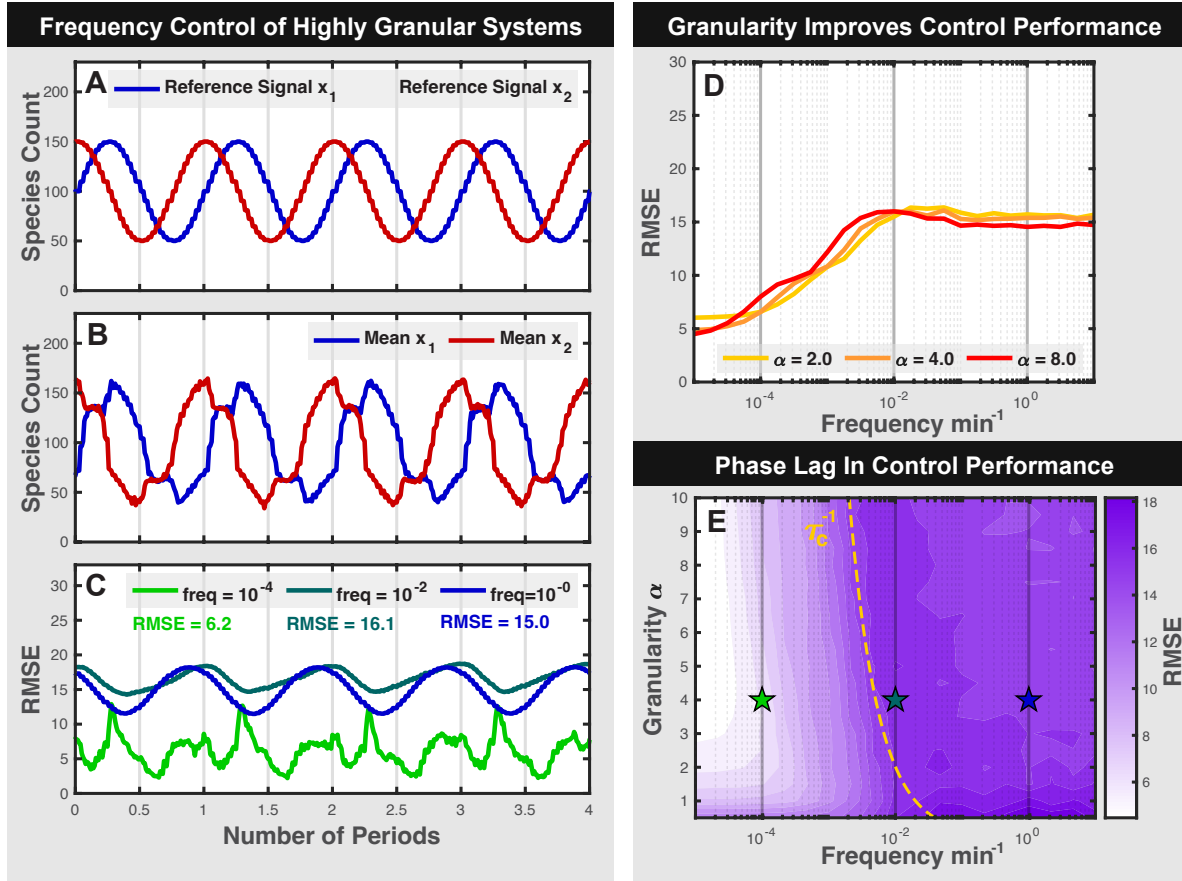
Figure 8. Control performance analyzed over a domain of f, α pairs show worst control performance at moderate frequencies near $1e - 2$ due to phase lag. Tracking reference signals when $\alpha = 5$ span a range between 50 and 150 species (A). Stochastic simulations driven using a phased lagged controller at $\alpha = 5$ and low frequency show tighter control compared to $\alpha = 1$ (B). Systems driven at moderate frequency show worse control performance than high frequency or low frequency (C). Control performance only of phase-lagged system only improves with increasing α and low f.

phases and frequencies (Figure 7D2). For all reference trajectories, the medians of the marginal distributions show good match with the desired reference signal (Figure 7B2,C2, and D2). To quantify the overall performance, Figs. 7(B3, C3,D3) show the root mean squared error as a function of time, and Figs. 7(B4, C4, and D4) show the time-averaged error distribution for the system response relative to the time varying target. From these figures, we observe that all trajectories result in short RMSE spikes at times, and these correspond to short, transient periods when the controller passes through the regions of poor control depicted in Figure. 6(E). Overall, the simulations show that the synchronous control performed best with an average RSME of 6.9. When the system is driven with a phase-lag, the average RSME of the score increases to 8.2, and when driven at a different frequency, the average RMSE goes up to 8.6.

In general, a given control system cannot effectively track a reference signal that changes faster that the system's natural time scale. Since it was shown that

increasing granularity (α) improves steady state control performance (Figure. 4G) but also lengthens this time scale (Figure. 4H), one should expect that these competing effects of granularity would also affect the types and speeds of signals to which the system can respond. To examine how driving frequency and system scale affects control performance, 64 SSA trajectories of the phase-separated dynamic controller were simulated over a two dimensional domain of points (α, f) for 32 cycles after reaching steady state. Figure 8(A) shows the desired reference signal for the system, and Figure 8(B) shows the mean of the system response when the frequency is $f = 10^{-4}min^{-1}$ Need units added them and the granularity is $\alpha = 4.0$. Figure 8(C) shows the corresponding control performance over normalized periodic time as α is held at 4.0 and f is increased from $f = 10^{-4}min^{-1}$ Units added them to $f = 10^{-2}min^{-1}$ Units added them to $f = 10^{-0}min^{-1}$ Units added them leading to average control performances of 6.2, 16.1, and 15.0 respectively. Figure 8D,E extends this analysis to plot the average control performance over different combinations of α and f. The characteristic frequency (given by the predicted τ_c^{-1} over a range of α) is plotted as the yellow dashed line. In particular, the heat map of control performance over (f, α) shows that the worst performance occurs at moderate f near $f = 10^{-2}min^{-1}$ and that control performance is best when granularity is high and frequency is low 8(E). Plots of the characteristic frequency given by the inverse of characteristic time 8(yellow line), show good match with the heat maps at high granularity but not at low granularity. These data When examining poorly performing trajectories at moderate frequencies, a phase lag was observed in the system. In this case, although the qualitative form of the response may match to the reference signal, this phase lag resulted in worse RMSE than no system response at all. At very large frequencies, the effect of the fast fluctuating control input is averaged, and the system barely responds.

try adding the line at $f = 1/tau_c = \gamma/(0.7 * \alpha)$ to this plot. Does it match the contours separating good and poor control? added τ_c^{-1}. using $\tau_c = 1/\gamma$

Go through every figure and make sure that the units are shown and that they are correct. If quantities are unitless, make sure that the form of the normalization is clearly expressed.

4. Conclusion

Key results from [1] showed that noise was a key requirement for the development of a noise-exploiting controller, and that deterministic systems could not be controlled to two different stable points if they both started at the same initial condition. As a stochastic system becomes increasingly more granular, it also becomes less noisy and more similar to its ODE solution which is known to be impossible to control to two different fates, but here, we have shown that the removal of noise through system granularity led to better control performance. Therefore, stochastic controllers may perform work best on models which are nearly deterministic, but not quite. Unfortunately, such systems were found to take longer time to achieve steady state.

The ability to analyze the model at one system granularity apply it elsewhere might help analyze models for which the computational effort may be too large. Since the computation time of the FSP solution to the CME grows with the square of the number of states, this can cause an explosion in computational requirements for large systems. One alternative is to learn a controller at a computationally feasible number of states and apply them to large systems which cannot be solves for using the FSP.

Parameter perturbation analysis showed that there is room to improve control performance by adjusting system parameters, and that joint optimization of the controller with the system parameters may lead to better control performance. It also shows that populations of cells where each cell might have its own parameter combination could still be reasonably controlled for small changes in parameter scale, but large changes could be detrimental.

Time delay analysis showed that increasing time delay decreased control performance. It was also found that a controller with less control information outperformed a controller with more information at higher levels of time delay. We believe this is happening because a controller with more information can afford to be more aggressive to implement its control, and time delay can cause this aggression to backfire. A controller was optimized which required no information in May et al which had a score of 402. This controller should be immune to time delay since no feedback is required for this controller. Here we saw both controllers did performed worse than 402 at very large time delay.

The control of cells to two slowly changing dynamic reference signals using a single global input by the use of a noise-exploiting controller showed good control performance for a variety of signals. These analysis could be extended to include faster frequency by numerical calculation or by alternative error-probability adjustments.

[1] M. May and B. Munsky, "Exploiting noise, nonlinearity, and feedback to differentially control multiple synthetic cells with a single optogenetic input," pp. 1–28, 2021. eps

[2] A. H. Ng, T. H. Nguyen, M. Gómez-Schiavon, G. Dods, R. A. Langan, S. E. Boyken, J. A. Samson, L. M. Waldburger, J. E. Dueber, D. Baker, and H. El-Samad, "Modular and tunable biological feedback control using a de novo protein switch," pp. 265–269, 2019.

[3] C. C. Liu, M. C. Jewett, J. W. Chin, and C. A. Voigt, "Toward an orthogonal central dogma," *Nature Chemical Biology*, vol. 14, no. 2, pp. 103–106, 2018.

[4] M. B. Sheets, W. W. Wong, and M. J. Dunlop, "Light-Inducible Recombinases for Bacterial Optogenetics," *ACS Synthetic Biology*, vol. 9, no. 2, pp. 227–235, 2020.

[5] T. M. Groseclose, R. E. Rondon, Z. D. Herde, C. A. Aldrete, and C. J. Wilson, "Engineered systems of inducible anti-repressors for the next generation of biological programming," *Nature Communications*, vol. 11, no. 1, pp. 1–15, 2020. [Online]. Available: http://dx.doi.org/10.1038/s41467-020-18302-1

[6] J. Shin, S. Zhang, B. S. Der, A. A. Nielsen, and C. A. Voigt, " Programming Escherichia coli to function as a digital display ," *Molecular Systems Biology*, vol. 16, no. 3, pp. 1–12, 2020.

[7] A. Baumschlager, S. K. Aoki, and M. Khammash, "Dynamic blue light-inducible T7 RNA polymerases (Opto-T7RNAPs) for precise spatiotemporal gene expression control," *ACS synthetic biology*, vol. 6, no. 11, pp. 2157–2167, 2017.

[8] S. Y. Chen, L. C. Osimiri, M. Chevalier, L. J. Bugaj, T. H. Nguyen, R. A. Greenstein, A. H. Ng, J. Stewart-Ornstein, L. T. Neves, and H. El-Samad, "Optogenetic Control Reveals Differential Promoter Interpretation of Transcription Factor Nuclear Translocation

Dynamics," *Cell Systems*, vol. 11, no. 4, pp. 336—-353.e24, 2020. [Online]. Available: http://dx.doi.org/10.1016/j.cels.2020.08.009

[9] G. Lillacci, Y. Benenson, and M. Khammash, "Synthetic control systems for high performance gene expression in mammalian cells," *Nucleic acids research*, vol. 46, no. 18, pp. 9855–9863, 2018.

[10] Z. R. Fox, S. Fletcher, A. Fraisse, C. Aditya, and S. Sosa, "MicroMator: Open and Flexible Software for Reactive Microscopy," *bioRxiv*, pp. 1–9, 2021. [Online]. Available: http://biorxiv.org/cgi/content/short/2021.03.12.435206v1

[11] A. Baumschlager and M. Khammash, "Synthetic Biological Approaches for Optogenetics and Tools for Transcriptional Light-Control in Bacteria," *Advanced Biology*, vol. 5, no. 5, p. 2000256, 2021. [Online]. Available: https://onlinelibrary.wiley.com/doi/abs/10.1002/adbi.202000256

[12] J. B. Lugagne, S. Sosa Carrillo, M. Kirch, A. Köhler, G. Batt, and P. Hersen, "Balancing a genetic toggle switch by real-time feedback control and periodic forcing," *Nature Communications*, vol. 8, no. 1, pp. 1–7, 2017. [Online]. Available: http://dx.doi.org/10.1038/s41467-017-01498-0

[13] M. Rullan, D. Benzinger, G. W. Schmidt, A. Milias-Argeitis, and M. Khammash, "An Optogenetic Platform for Real-Time, Single-Cell Interrogation of Stochastic Transcriptional Regulation," *Molecular Cell*, vol. 70, no. 4, pp. 745–756.e6, 2018. [Online]. Available: https://doi.org/10.1016/j.molcel.2018.04.012

[14] A. Guarino, D. Fiore, D. Salzano, and M. Di Bernardo, "Balancing Cell Populations Endowed with a Synthetic Toggle Switch via Adaptive Pulsatile Feedback Control," *ACS Synthetic Biology*, vol. 9, no. 4, pp. 793–803, 2020.

[15] B. Munsky, G. Neuert, and A. Van Oudenaarden, "Using gene expression noise to understand gene regulation," *Science*, vol. 336, no. 6078, pp. 183–187, 2012.

[16] P. Szymańska, N. Gritti, J. M. Keegstra, M. Soltani, and B. Munsky, "Using noise to control heterogeneity of isogenic populations in homogenous environments," *Physical Biology*, vol. 12, no. 4, 2015.

[17] D. T. Gillespie, "A rigorous derivation of the chemical master equation," *Physica A: Statistical Mechanics and its Applications*, vol. 188, no. 1-3, pp. 404–425, 1992.

[18] D. T. Gillespie, "Exact stochastic simulation of coupled chemical reactions," *The journal of physical chemistry*, vol. 81, no. 25, pp. 2340–2361, 1977.